npj | Quantum Information

www.nature.com/npjqi

ARTICLE OPEN

Check for updates

Highly tunable magneto-optical response from magnesium-vacancy color centers in diamond

Anton Pershin[1], Gergely Barcza[1], Örs Legeza[1,2] and Adam Gali[1,3]✉

Defect quantum bits (qubits) constitute an important emerging technology. However, it is necessary to explore new types of defects to enable large-scale applications. In this article, we examine the potential of magnesium-vacancy (MgV) in diamond to operate as a qubit by computing the key electronic- and spin properties with robust theoretical methods. We find that the electronic structure of MgV permits the coexistence of two loosely separated spin-states, where both can emerge as a ground state and be interconverted depending on the temperature and external strain. These results demonstrate a route to control the magneto-optical response of a qubit by modulating the operational conditions.

npj Quantum Information (2021)7:99 ; https://doi.org/10.1038/s41534-021-00439-6

INTRODUCTION

Control over the formation of defects is vital for many emerging areas of physics, chemistry, and materials science, from electronics to photocatalysis. Although defects generally tend to deteriorate the properties of the host material, with a rational design, these impurities can play a key role in engineering desirable properties, such as a high conductivity via doping or in boosting catalytic activity, e.g., for water splitting[1,2]. Moreover, some defects, also known as color centers, result in the formation of new states inside the band gap. As the electronic levels of color centers are well-separated from the band edges of the semiconductor host materials, they constitute a platform for the practical implementation of quantum bits (qubits)[3,4]. In turn, the capability to store and process quantum information with the localized defect spin states permits realization of various next-generation technologies, such as quantum computers, quantum memory, and quantum sensors[5,6].

In practice, building up the necessary high-fidelity networks of defect qubits is challenging owing to their rapid decoherence, caused by spin-lattice interactions in the presence of nuclear spins[7]. Negatively charged nitrogen-vacancy center [NV(−)] in diamond represents the most studied defect qubit to date. However, the simple optical readout of the NV(−) spin state is inefficient, while an improvement over the signal-to-noise ratio requires specialist techniques[8–10]. Moreover, near-surface NV(−) centers (needed for quantum sensing) are unstable to the commonly used types of surface termination. This compromises the fidelity and also reduces the spin-coherence time compared with their bulk counterparts, which in turn affects the spectral resolution[11]. Furthermore, to enable applications in bioimaging and quantum communication, longer wavelengths are typically needed than the zero-phonon line (ZPL) of the lowest optically allowed transition at 637 nm (1.945 eV)[12]. Indeed, the signal from the NV(−) center can successfully be downconverted, even reaching telecommunication wavelengths (1588 nm), but this comes at the expense of the loss in quantum efficiency (which drops to ≤17%) and the requirement of a complex optical setup[13]. In addition, for quantum communication, coherent emission from ZPL is required, which is difficult to achieve with the NV(−) center as the Debye–Waller factor is only 0.03[14].

Although many of the bottlenecks mentioned above can be largely overcome with both involved optical protocols and material processing, they have also motivated the search for new defect configurations with an improved magneto-optical response in terms of quantum efficiency, Debye–Waller factor, radiation lifetime, and spectral diffusion[15–17]. For instance, the SiV center is recognized for stable and bright emission, and a large Debye–Waller factor of 0.7[18]; these properties can be attributed to its inversion symmetry. The other group-IV-vacancy complexes, including SnV, PbV, and GeV[17,19], offer a further improvement on the coherence time, relative to SiV, owing to a larger separation of the spin levels (see a recent review for the properties of these and other color centers in diamond[20]). As a part of the screening for new optical centers in diamond, Lühmann et al.[21] identified a Mg-related center with a bright and mostly coherent emission. Of particular note, no optically detected magnetic resonance was found for this defect in the frequency range from 0.5 to 4 GHz. Further investigation by the same authors revealed that the defect exhibits a remarkable photostability[22]. Thus, a pronounced ZPL at 557 nm (2.23 eV, originating from the defect states) remains surprisingly stable in the entire range of Fermi-level positions, as controlled by boron- and phosphorous doping of diamond. This feature distinguishes the Mg-related center from most of the point defects in diamond, where the target charge/spin states are found within a narrow energy window relative to the position of Fermi level. Based on the measured polarization of absorption, the authors tentatively assigned the photoluminescence (PL) feature to a magnesium-vacancy (MgV) complex; however, the charge- and spin state of the complex as well as the possibility to operate as a qubit have not yet been determined.

In this work, we carry out a robust theoretical investigation to assess the role of Mg in the formation of color centers in diamond, with an aim to identify the origin of the experimentally observed photostable ZPL signal at 2.23 eV. Starting with evaluating the formation energies and by computing the optical properties, we show that MgV is the most stable simple defect configuration with a photostable −1 charge state. We further compute the PL response in the doublet spin-manifold; found to be in excellent agreement with the experimental observations. Moreover, we demonstrate that MgV(−) center possesses an electronic structure that enables coexistence of several bright transitions, including

[1]Wigner Research Centre for Physics, PO Box 49, Budapest, Hungary. [2]Fachbereich Physik, Philipps-Universität Marburg, D-35032 Marburg, Germany. [3]Department of Atomic Physics, Budapest University of Technology and Economics, Budapest, Hungary. ✉email: gali.adam@wigner.hu

Published in partnership with The University of New South Wales

npj nature partner journals

those at longer wavelengths, which have not been experimentally identified. We also show potential routes towards the stabilization of other emission signals through a rational control of operational and preparation conditions, such as temperature and applied strain. Our findings therefore pave the way towards highly-efficient qubits with the operational wavelengths, particularly suitable for biological applications.

RESULTS AND DISCUSSION

Electronic and thermodynamic properties of Mg color centers

To identify the origin of the experimental PL signal, we first compare the electronic structures of four simple defect configurations involving Mg: interstitial and substitutional Mg; MgV; and MgV_2. The electronic structures computed by HSE06, shown in Supplementary Figs. 1b, 2, demonstrate that in each case, incorporation of Mg into the diamond lattice leads to the development of photoactive localized states inside the band gap. However, the energy gap between the highest occupied- and lowest unoccupied-localized levels for the respective most stable charge states (see Supplementary Fig. 3) do not exceed 1.5 eV, which provides a first indication for the lowest transition energy when neglecting excitonic effects. In particular, irrespective of the charge state of MgV, the difference between the e_u and e_g Kohn–Sham energies (which are responsible for a ZPL of SiV center in diamond[23]) is much smaller than 2.23 eV; the energy at which ZPL was experimentally identified. Of note, in the low spin-0 configurations, a small energy separation between the frontier orbitals in MgV(0) promotes strong correlation effects, as further verified by the density matrix renormalization group (DMRG) calculations (see Supplementary Table 1). However, the resulting increase in the optical gap is still not sufficient to explain the ZPL at 2.23 eV. Our findings thus suggest that for MgV to be the experimentally observed color center, a higher lying electronic transition, likely involving the deeper localized a_{2u} orbital, should give rise the PL signal; this would be at odds with the Kasha's rule. It also appears that the substitutional Mg is another possible source of the green emission. In the following, however, we show that this defect cannot demonstrate photostability over a large energy range and is also less thermodynamically favorable than MgV.

The formation energies of the four Mg centers in diamond as a function of Fermi energy are shown in Fig. 2. Here, none of the four centers exhibit a single charge state within the band gap that could explain the photostability of the ZPL. Therefore, to be maintained for a sufficiently large energy window, the photostability should originate from photoionization, where the laser pulse of 2.33 eV continuously promotes electrons from (to) the valence (conduction) band, thereby stabilizing a unique charge state. In terms of the absolute values of the formation energy, MgV is the most stable among the four considered defects, whereas the positions of charge transition levels are favorable for the optical stabilization of MgV(−) center. Note that the formation energy of MgV decreases with accumulating the negative charge, which also contributes to a more intense emission—as observed experimentally for the n-type doping condition—due to larger defect density. Considering that the formation energy of a single vacancy in diamond is ~7 eV[24,25], the surprising stabilization of MgV over a substitutional Mg defect points to a weak (repulsive) interaction between the Mg ion and carbon lattice. This is further confirmed by artificially dispositioning Mg and V, as shown in Supplementary Fig. 4, resulting in the stabilization of the adjacent configuration by ~9 eV irrespective of the charge state; therefore, thermal annealing ultimately drives the substitutional Mg to form MgV complexes. In turn, photoionization cannot explain the photostability for substitutional Mg: the non-emissive (due to full occupation of the t_2 levels) −2 charge state appears above the ionization threshold by ~0.4 eV, while photostability of a single charge state from the remaining +1, 0, and −1 would involve multi-electron transitions, which are unlikely to take place.

Magneto-optical properties of the MgV defect

Having identified the MgV defect as the best candidate for the origin of the 2.23 eV emission, we focus on the analysis of the electronic structure and spin properties of MgV complexes. As shown in Fig. 1b, the presence of MgV(−) center in diamond gives rise to the appearance of five localized orbitals (a_{2u}, e_u, and e_g) close to the Fermi level. However, in stark contrast to the group-IV elements—vacancy centers, the proximity of e_u and e_g allows for the coexistence of two loosely separated doublet- and (high-spin) quartet states, in line with the results for MgV(0) (see Supplementary Table 4). Moreover, as computed from the HSE06 adiabatic potential energy surfaces, the quartet ^4E_u appears as a ground state with a stabilization energy of 37 meV over the doublet ^2E_g at the high symmetry point. Note that both ^4E_u and ^2E_g states are prompted to undergo the Jahn-Teller (JT) distortion, resulting in a symmetry reduction to C_{2h} upon the 2 + 4 relaxation scenario (two of six C-Mg bonds become shorter than the remaining four) with the JT energies of 60 and 70 meV, respectively. Furthermore, owing to small offset between ^4E_u and ^2E_g energies, the electron–phonon interaction also interferes with the alignment of the spin states. Following the methodology from ref. [19] we corrected the adiabatic energies for the effect of electron–phonon coupling, and found the true vibronic JT energies of 97 and 84 meV for the doublet- and quartet state, respectively, giving the final energy difference between the two states of 22 meV. Hence, the thermal energy (~27 meV at 300 K)

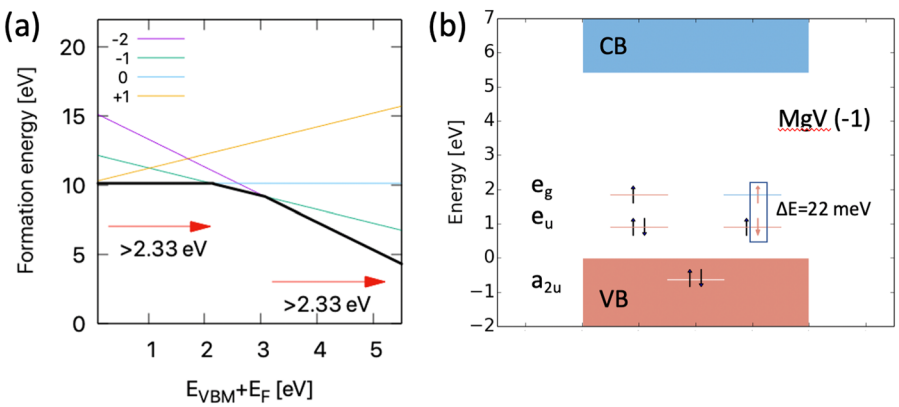

Fig. 1 Ground state properties of MgV color center in diamond. a A formation energy diagram for the MgV defect, where 2.33 eV indicates the energy of the green laser pulse. **b** A schematic representation of the electronic structure for the MgV(−). Here, the coexistence of two possible ground states, separated by 22 meV, is depicted by a respective spin-flip process.

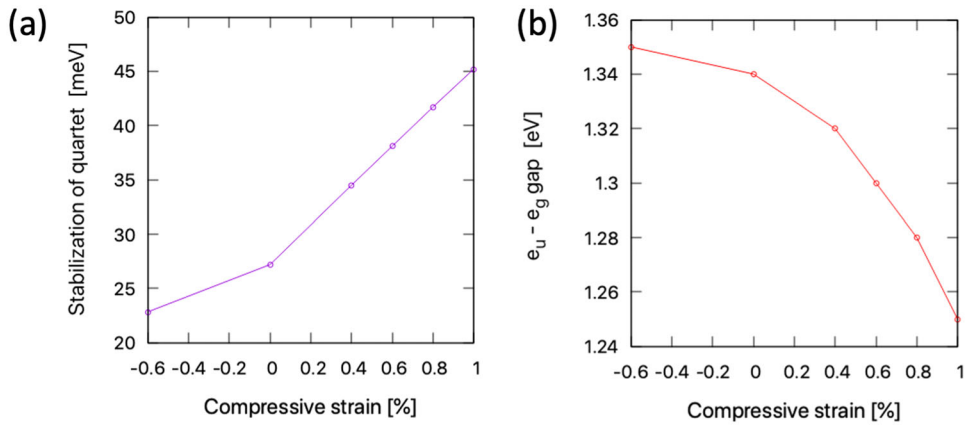

Fig. 2 Modifications of the electronic structure due to the applied strain. a Stabilization of the quartet ground state over doublet as a function of applied compressive strain, computed at the HSE06 adiabatic potential energy surfaces, including the relaxation effects, together with **b** the respective modifications of the e_u–e_g gap in the spin-up channel.

should be sufficient to enable the spin-conversion to the higher lying doublet state.

In addition, in Fig. 2 we show another route for controlling the spin properties of the ground state that is based on applying an external strain along (100) direction. Here, we demonstrate that the uniaxial compressive strain reduces the energy of the ^4E_u ground state, which in turn hinders the population of ^2E_g at room temperature. This effect can be understood from the difference in electronic structure, where we observe a decrease in the e_u–e_g gap energy as a function of compressive strain, which then stabilizes the high-spin solution. However, the strength of effect saturates when close to the equilibrium (zero-strain) structure, yielding a smaller modification in the opposite direction. Hence, rather large values of the tensile strain are needed to enable the crossover, although it allows the possibility for the thermal occupation of ^2E_g. We note that such a small energy separation between two spin states, which ultimately allows for the temperature control and strain engineering of the nature of ground state, was not reported for point defects in diamond.

Next, we addressed the optical properties of the MgV(−) center, focusing on both spin-manifolds. We first computed the (vertical) absorption spectra for our cluster model by employing the complete active space self-consistent field (CASSCF) method. As shown in Fig. 3a and Supplementary Table 5, in the energy window below 3 eV, each ^4E_g and ^2E_u state features two bright transitions where the excitation energies are separated by ~1.5 eV. The two lowest ^4E_u and ^2E_g are solely formed by promoting the electrons from e_u to e_g orbitals and are found at ~0.7 and ~1.1 eV, respectively, both considerably smaller than the experimental PL signal. As follows from the analysis of the CASSCF wavefunction, the $^4A_{2g}$ state at 2.7 eV is governed by a single Slater determinant that justifies the application of ΔSCF method in the bulk model, resulting in the ZPL of ~2.8 eV. The complete state energy diagram obtained by the ΔSCF method is shown in Fig. 3b, while the respective CASSCF results are depicted in Supplementary Fig. 1b. In order to enhance the stability of the ΔSCF calculations for the ^2E_u states, we considered the photoionization scenario from −2 charge state (see Supplementary Fig. 5), which also enables the method to perform best due to the absence of a strong correlation. Altogether, our findings suggest that $^2E_u^{(2)}$–^2E_g excitation is responsible for the experimentally observed PL signal. To further confirm this, we have computed the phonon sideband associated with this transition. The resulting theoretical spectrum, shown in Fig. 3c, is in excellent agreement with experiment, reproducing both the position of ZPL (at 2.2 eV by the HSE calculations) and its vibronic replicas. As shown in Table 1, our calculations indicate a large value of the associated oscillator strength (f_{osc}) of $\sim 2 \times 10^{-1}$, originating from the transition dipole moment (μ) of 3.4 D. Moreover, owing to the small reorganizations in the excited state, the resulting Debye–Waller factor was found to be 0.54. Note that a small difference between the two spectra at energies below ~2 eV is associated with the presence of another weakly-allowed transition between $^2A_{1u}$ and ^2E_g ($f_{osc} = 5 \times 10^{-2}$) that contributes to the enhancement of the experimental sideband. In turn, the violation of Kasha's rule can be understood by reduced nonradiative decay rate between the ^2E_u and $^2E_u^{(2)}$ excited states with respect to that of other non-inversion symmetric color centers in diamond because of the parity selection rules[26]. A similar argument holds for the transition between $^2E_u^{(2)}$ and $^2A_{1u}$; therefore, once the system is optically initialized in the $^2E_u^{(2)}$, the radiative transition to the ground state becomes the most favorable deactivation pathway.

Finally, our identification of the ^2E_g as a ground state in the experiment is consistent with the absence of an ODMR signal below 4 GHz[21]. Instead, splitting between the levels is expected owing to the spin-orbit interaction, as observed for the group-IV elements—vacancy centers in diamond[19]. For MgV(−), we computed an intrinsic splitting of 220 GHz, which reduces to 30 GHz due to the dynamic JT effect. We note that the intrinsic spin-orbit value was calculated in our 512-atom supercell calculations and will provide a good estimate for the order of magnitude[19]. The appearance of this resonance illustrates the potential of MgV(−) to operate as a qubit, while the estimated splitting in the spin levels of about few tenth of GHz is an order of magnitude larger than the one applied in the above mentioned measurements[21]. Nevertheless, the spin-selective population of the states may be achieved by a quantum optical protocol, as already demonstrated for a similar system[27].

To conclude, we have performed an extensive theoretical investigation to elucidate the role of Mg in the formation of color centers in diamond. Our calculations reveal that MgV is the most stable defect configuration among those considered, with a photostable −1 charge state, achieved in experiment by photoionization with a green laser. Furthermore, we showed that this defect feature possesses an inversion symmetry and emits light from the third bright excited state, at odds with Kasha's rule. It also possesses quasi-degenerate quartet and doublet ground states, each of them exhibiting distinct photophysical properties. Although we have assigned the experimental PL signal to the $^2E_u^{(2)}$–^2E_g transition, the quartet state (which appeared to be in thermal equilibrium with the doublet ^2E_g) has ZPL of ~1.1 eV, lying in the near-infrared window in biological tissue.

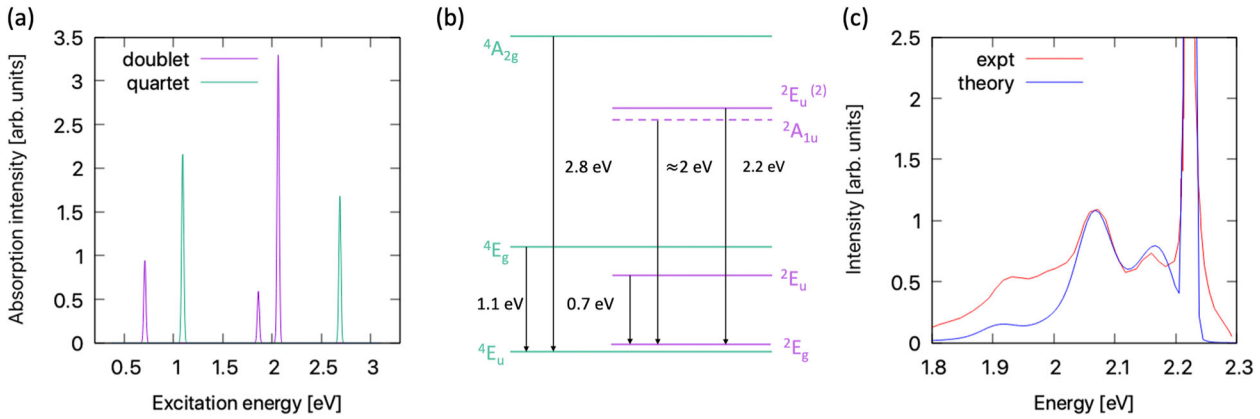

Fig. 3 Optical properties of MgV(−). a The CASSCF vertical absorption spectra from both ground states of MgV(−). **b** A respective state energy diagram as deduced by ΔSCF method using HSE06 functional for the bright electronic transitions. Here, $^2A_{1u}$ state is positioned according to the CASSCF energy gap between ^2A_u and $^2E_u^{(2)}$ while omitting the structural relaxation. **c** HSE06 phonon sideband for the $^2E_u^{(2)}$–^2E_g transition, overlapped with the experimental PL signal from the Mg color center (experimental data is from ref. [11]).

Table 1. Summary of the major finding for the MgV(−) defect.

Property	Value
Charge transition levels	
0/−1	2.1 eV[a]
−1/−2	3.1 eV[a]
Ground state	
^2E_g–^4E_u energy gap	22 meV[a]
Magneto-optical properties	
ZPL of $^2E_u^{(2)}$–^2E_g	2.2 eV[a]
f_{osc}	0.2[b]
Transition dipole moment	3.4 D[b]
Debye–Waller factor	0.54[a]
Spin-orbit splitting, λ_0	220 GHz[a]
Reduction factor, p	0.14[a]
λ_0	30.8 GHz[a]

Most of the properties, including the positions of charge transition levels, ^2E_g–^4E_u energy gap when taking into account the electron–phonon coupling, and magneto-optical properties were computed by HSE06. The transition dipole moment and f_{osc} were deduced from the CASSCF calculations.
[a]Computed by DFT.
[b]Computed by CASSCF.

METHODS

Density functional theory calculations

The optimized geometries and electronic structures of four Mg color centers, shown in Supplementary Figs. 1, 2, were computed with the HSE06 density functional[28] utilizing the projector-augmented wave method with the kinetic energy cutoff of 400 eV. The calculation for Mg atoms, incorporated into the 512-carbon supercell were performed with VASP package[29]. The ZPL together with the phonon sideband were computed by ΔSCF method[30]. Thermodynamic stability of each defect configuration was evaluated based on the formation energies as a function of Fermi energy (E_F), given as[14]:

$$E^q_{\text{form}}(E_F) = E^q_{\text{total}}(C512 : defect) - n_C\mu_C - \mu_{\text{Mg}} + q(E_F + E_{\text{VBM}}) + E^q_{\text{corr}}, \quad (1)$$

where E^q_{total} is the total energy of the system in a charge state q, μ_C, and μ_{Mg} are chemical potentials of C and Mg, respectively, n_C is a number of carbon atoms in the supercell, E_{VBM} is the calculated position of the valence band maximum in diamond. E^q_{corr} is the charged defect correction, which was computed by SXDEFECTALIGN code implementing the Freysoldt correction scheme[31].

DMRG calculations

Many-body electronic excitation spectrum was computed using the DMRG approach[32] applied on top of periodic Kohn–Sham orbitals[33]. DFT and DMRG simulations were performed using the Quantum Espresso[34,35], and the Budapest DMRG package[36], respectively. The two program suites are interfaced using our in-house developed code, which constructs the Hamiltonian of the active orbitals corresponding to the CAS method[37,38]. Active space includes orbitals around the Fermi surface. The accuracy of the DMRG calculations is controlled by the dynamic block state selection approach and the computational efficiency is improved by initialization procedures, which are inspired by quantum information theoretical considerations[39]. Investigating multiple excitations, distinct DMRG calculations are performed for target states of different total spin. Spin-restricted Kohn–Sham orbitals for generating CAS are optimized by smearing the electron pair with highest energy and the unpaired electron evenly on the partially occupied degenerate e-orbitals for MgV(0) and for MgV(−), respectively. These calculations were performed for the 216-atom model of diamond using norm-conserving pseudopotentials with a kinetic energy cutoff of 680 eV for the DFT part.

CASSCF calculations

For the MgV defect, the CASSCF method was further employed to treat the highly correlated states, based on a cluster of 84 C-atom (see Supplementary Fig. 1) as implemented in ORCA code[40]. Here, the strong correlation effects are incorporated by solving the full-CI problem for a set of active orbitals, which is formulated on top of the reference (Hartree–Fock) wavefunctions. In our CASSCF calculations, we employed the cc-pVDZ basis set[41] and used five localized active orbitals (see Fig. 1b) occupied by an appropriate number of electrons (from 6 to 8), depending on the target charge state of MgV. Note that although CASSCF and DMRG are rather two distinct methods, DMRG may be viewed as an extension of CASSCF towards exploring larger active spaces (see ref. [42] and references therein).

DATA AVAILABILITY

All data sets are available from the corresponding author upon reasonable request.

Received: 15 February 2021; Accepted: 27 May 2021;
Published online: 18 June 2021

REFERENCES

1. Queisser, H. J. & Haller, E. E. Defects in semiconductors: some fatal, some vital. *Science* **281**, 945 (1998).
2. Liu, J., Wei, Z. & Shangguan, W. Defects engineering in photocatalytic water splitting materials. *ChemCatChem* **11**, 6177 (2019).
3. Weber, J. R. et al. Quantum computing with defects. *Proc. Natl Acad. Sci. USA* **107**, 8513 (2010).

4. Awschalom, D. D., Bassett, L. C., Dzurak, A. S., Hu, E. L. & Petta, J. R. Quantum spintronics: engineering and manipulating atom-like spins in semiconductors. *Science* **339**, 1174 (2013).
5. Wehner, S., Elkouss, D., and Hanson, R. Quantum internet: a vision for the road ahead. *Science* **362**, 6412 (2018).
6. Pezzagna, S. & Meijer, J. Quantum computer based on color centers in diamond. *Appl. Phys. Rev.* **8**, 011308 (2021).
7. Balasubramanian, G. et al. Ultralong spin coherence time in isotopically engineered diamond. *Nat. Mater.* **8**, 5 (2009).
8. Irber, D. M. et al. Robust all-optical single-shot readout of nitrogen-vacancy centers in diamond. *Nat. Commun.* **12**, 1 (2021).
9. Shields, B. J., Unterreithmeier, Q. P., de Leon, N. P., Park, H. & Lukin, M. D. Efficient readout of a single spin state in diamond via spin-to-charge conversion. *Phys. Rev. Lett.* **114**, 136402 (2015).
10. Robledo, L. et al. High-fidelity projective read-out of a solid-state spin quantum register. *Nature* **477**, 574 (2011).
11. Findler, C., Lang, J., Osterkamp, C., Nesládek, M. & Jelezko, F. Indirect overgrowth as a synthesis route for superior diamond nano sensors. *Sci. Rep.* **10**, 1 (2020).
12. Davies, G. & Hamer, M. F. Optical studies of the 1.945 ev vibronic band in diamond. *Proc. R. Soc. Lond. A.* **348**, 285 (1976).
13. Dréau, A., Tcheborateva, A., Mahdaoui, A. E., Bonato, C. & Hanson, R. Quantum frequency conversion of single photons from a nitrogen-vacancy center in diamond to telecommunication wavelengths. *Phys. Rev. Appl.* **9**, 064031 (2018).
14. Gali, Á. Ab initio theory of the nitrogen-vacancy center in diamond. *Nanophotonics* **8**, 1907 (2019).
15. Christle, D. J. et al. Isolated spin qubits in sic with a high-fidelity infrared spin-to-photon interface. *Phys. Rev. X* **7**, 021046 (2017).
16. Pingault, B. et al. Coherent control of the silicon-vacancy spin in diamond. *Nat. Commun.* **8**, 1 (2017).
17. Bradac, C., Gao, W., Forneris, J., Trusheim, M. E. & Aharonovich, I. Quantum nanophotonics with group iv defects in diamond. *Nat. Commun.* **10**, 1 (2019).
18. Aharonovich, I. et al. Diamond-based single-photon emitters. *Rep. Prog. Phys.* **74**, 076501 (2011).
19. Thiering, G. & Gali, A. Ab initio magneto-optical spectrum of group-iv vacancy color centers in diamond. *Phys. Rev. X* **8**, 021063 (2018).
20. Thiering, G. and Gali, A. *Chapter One - Color Centers in Diamond for Quantum Applications, in Semiconductors and Semimetals*. (eds. C. E. Nebel, I. Aharonovich, N. Mizuochi, and M. Hatano) Vol. **103**, pp. 1–36 (Elsevier, 2020).
21. Lühmann, T. et al. Screening and engineering of colour centres in diamond. *J. Phys. D: Appl. Phys.* **51**, 483002 (2018).
22. Lühmann, T., John, R., Wunderlich, R., Meijer, J. & Pezzagna, S. Coulomb-driven single defect engineering for scalable qubits and spin sensors in diamond. *Nat. Commun.* **10**, 1 (2019).
23. Gali, A. & Maze, J. R. Ab initio study of the split silicon-vacancy defect in diamond: electronic structure and related properties. *Phys. Rev. B* **88**, 235205 (2013).
24. Shim, J., Lee, E.-K., Lee, Y. J. & Nieminen, R. M. Density-functional calculations of defect formation energies using supercell methods: defects in diamond. *Phys. Rev. B* **71**, 035206 (2005).
25. Bourgoin, J. C. An experimental estimation of the vacancy formation energy in diamond. *Radiat. Eff.* **79**, 235 (1983).
26. Burshtein, Z. Radiative, nonradiative, and mixed-decay transitions of rare-earth ions in dielectric media. *Opt. Eng.* **49**, 091005 (2010).
27. Sukachev, D. D. et al. Silicon-vacancy spin qubit in diamond: a quantum memory exceeding 10 ms with single-shot state readout. *Phys. Rev. Lett.* **119**, 223602 (2017).
28. Krukau, A. V., Vydrov, O. A., Izmaylov, A. F. & Scuseria, G. E. Influence of the exchange screening parameter on the performance of screened hybrid functionals. *J. Chem. Phys.* **125**, 224106 (2006).
29. Kresse, G. & Furthmüller, J. Efficient iterative schemes for ab initio total-energy calculations using a plane-wave basis set. *Phys. Rev. B* **54**, 11169 (1996).
30. Gali, A., Janzén, E., Deák, P., Kresse, G. & Kaxiras, E. Theory of spin-conserving excitation of the n-v- center in diamond. *Phys. Rev. Lett.* **103**, 186404 (2009).
31. Freysoldt, C., Neugebauer, J. & Van de Walle, C. G. Fully ab initio finite-size corrections for charged-defect supercell calculations. *Phys. Rev. Lett.* **102**, 016402 (2009).
32. White, S. R. Density matrix formulation for quantum renormalization groups. *Phys. Rev. Lett.* **69**, 2863 (1992).
33. Barcza, G. et al. DMRG on top of plane-wave kohn–sham orbitals: a case study of defected boron nitride. *J. Chem. Theory Comput.* **17**, 1143 (2021).
34. Giannozzi, P. et al. Advanced capabilities for materials modelling with QUANTUM ESPRESSO. *J. Phys. Condens. Matter* **29**, 465901 (2017).
35. Giannozzi, P. et al. QUANTUM ESPRESSO: a modular and open-source software project for quantum simulations of materials. *J. Phys. Condens. Matter* **21**, 395502 (2009).
36. Legeza, Ö., Veis, L., and Mosoni, T. *QC-DMRG-Budapest, a Program for Quantum Chemical DMRG Calculations* (HAS RISSPO Budapest, 2000).
37. Cramer, C. J. *Essentials of Computational Chemistry: Theories and Models* (Wiley, 2005).
38. Jensen, F. *Introduction to Computational Chemistry* (John Wiley and Sons, Inc., 2006).
39. Szalay, S. et al. Tensor product methods and entanglement optimization for ab initio quantum chemistry. *Int. J. Quant. Chem.* **115**, 1342 (2015).
40. Neese, F. Software update: the ORCA Program System, Version 4.0, Wiley Interdiscip. *Rev. Comput. Mol. Sci.* **8**, e1327 (2018).
41. Dunning, T. H. Gaussian basis sets for use in correlated molecular calculations. i. The atoms boron through neon and hydrogen. *J. Chem. Phys.* **90**, 1007 (1989).
42. Nakatani, N. & Guo, S. Density matrix renormalization group (DMRG) method as a common tool for large active-space CASSCF/CASPT2 calculations. *J. Chem. Phys.* **146**, 094102 (2017).

ACKNOWLEDGEMENTS

The authors are thankful to Dr. Gergő Thiering, professor Christoph Becher, and Dr. Alexander Gillett for the useful discussions. This work was supported by the Ministry of Innovation and Technology and the National Research, Development and Innovation Office of Hungary (NKFIH) within the Quantum Information National Laboratory of Hungary, the National Quantum Technology Program (NKFIH Grant no. 2017-1.2.1-NKP-2017-00001). A.G. acknowledges the National Excellence Program (NKFIH Grant no. KKP129866), the EU QuantERA project "Q_magine" (NKFIH Grant no. 127889) as well as the support of the European Commission within the Quantum Technology Flagship Project ASTERIQS (Grant no. 820394). G.B. acknowledges support of the NKFIH PD-17-125261, the NKFIH FK-20-135496 projects and of the Bolyai Research Scholarship of the Hungarian Academy of Sciences. O.L. acknowledges support of the NKFIH K120569 and K134983. The development of the DMRG libraries was supported by the Center for Scalable and Predictive methods for Excitation and Correlated phenomena (SPEC), which is funded from the Computational Chemical Sciences Program by the U.S. Department of Energy (DOE), at the Pacific Northwest National Laboratory.

AUTHOR CONTRIBUTIONS

A.G. initiated and supervised the work. A.P. designed and implemented DFT and CASSCF parts of the project. B.G. and O.L. performed DMRG calculations. A.P. and A.G. wrote the paper with input from all authors. All authors discussed the results and contributed to the final manuscript.

COMPETING INTERESTS

The authors declare no competing interests.

ADDITIONAL INFORMATION

Supplementary information The online version contains supplementary material available at https://doi.org/10.1038/s41534-021-00439-6.

Correspondence and requests for materials should be addressed to A.G.

Reprints and permission information is available at http://www.nature.com/reprints

Publisher's note Springer Nature remains neutral with regard to jurisdictional claims in published maps and institutional affiliations.